Mechanosensitivity of an ABC Membrane Transporter Revealed by Single Molecule FRET and Activity Measurement

Alicia Damm[1‡], Su-Jin Paik[1‖§], Raj Kumar Sadhu[1§], Aurélie Di-Cicco[1], John Manzi[1], Michele Castellana[1], Emmanuel Margeat[2], Maxime Dahan[1†], Pierre Sens[1], Daniel Lévy[1]*, Patricia Bassereau[1]*

[1] Institut Curie, Université PSL, Sorbonne Université, CNRS UMR168, Physique des Cellules et Cancer, 75005 Paris, France

[2] Centre de Biologie Structurale (CBS), Université Montpellier, CNRS, INSERM, Montpellier, France

‡ Present address: Laboratoire de Physique de l'Ecole Normale Supérieure, ENS, Université PSL, CNRS UMR 8023, Sorbonne Université, Université de Paris, F-75005 Paris, France

‖ Present address: Imagine Institute, Paris, France

§ Equally contributed

*Correspondence to: Daniel Lévy (daniel.levy@curie.fr) and Patricia Bassereau (patricia.bassereau@curie.fr)

Abstract

While mechanosensitive ion channels' gating has been well documented, the effect of membrane mechanics, in particular membrane curvature, on the function of transporters remains elusive. Since conical shape transmembrane proteins locally deform membranes, conversely membrane bending could impact their conformations and their function. We tested this hypothesis using BmrA, a bacterial ABC exporter that exhibits large conformational changes upon ATP hydrolysis, switching between open and closed states with opposite V-shapes. After reconstitution in liposomes of controlled curvature, we showed that BmrA ATPase activity decreases by 2.9-fold when their diameter decreases from 125 to 29 nm. Moreover, using single-molecule FRET, we observed that the fraction of closed conformations is significantly reduced in highly curved vesicles when adding ATP or non-hydrolysable AMP-PNP. Our results are well explained by a theoretical 2-states model including the effect of membrane mechanics on protein shape transition. Our work reveals that the functional cycle of conical transporters is curvature sensitive, to an extent depending on protein geometry.

Teaser

High membrane curvature strongly impacts the functional cycle of transporters

MAIN TEXT

Introduction

Transmembrane proteins, being embedded in cell membranes, are prone to react to continuous mechanical deformations due to remodeling and stresses applied to the lipid bilayers. Cells use a large family of proteins, the mechanosensitive channels, to control the permeability of their membrane in response to mechanical stresses. This is the case with the eukaryotic ion channels Piezo[1,2], TRAAK/TREK1[3], and with the prokaryotic Msc family[4], that open at high membrane stretching and allow ions to flow through. It has also been proposed on theoretical basis that these channels could also be sensitive to local high membrane curvature (higher than about 1/50 nm)[5,6], which was confirmed with the Piezo channel[1,7]. The effect of membrane curvature is expected to be enhanced for proteins with an asymmetrical (conical) shape[5], that locally deform membranes[8,9]. Interestingly, some studies have revealed mechanosensitivity upon stretching of proteins with other identified functions, such as the voltage-gated channel KvAP[10]. In fact KvAP has a conical shape[11,12] and locally bends the bilayer[9,13], but only the effect of membrane tension on its function has been explored. We expect that other conical transmembrane proteins are potentially mechanosensitive to membrane curvature. Among them, a sub-group of ABC transporters (ATP-Binding Cassette), known as type IV exporters. These transporters have a domain-swapped arrangement with a V-shape, and are known to be flexible trans-membrane proteins that undergo large conformational changes within the bilayer[14–17]. Moreover, they could locally deform membranes, according to numerical simulations on the human ABC Pgp[9]. These transporters are thus good candidates to test this mechanosensitivity property.

ABC transporters are ubiquitous proteins present in organisms from bacteria to human. They hydrolyze ATP for the transport of a plethora of substrates such as drugs, lipids, ions, peptides (reviewed in [15,18]). They share a commune topology with two transmembrane domains (TMD), two nucleotide-binding sites (NBD) and two intracytoplasmic domains that join TMDs and NBDs. The structure and function of ABCs have been extensively investigated. Type IV ABCs, such as the bacterial lipid exporter MsbA, the Pgp human multidrug resistance protein, or the non-exporter gated chloride channel CFTR, have a "V-shape" apo-conformation and undergo significant conformational changes during their function. A simplified transport mechanism generally involves a two-state mechanism (Fig. 1A): ATP binding to the NBDs induces their dimerisation and switching of the protein from an "open" state - also called "apo"- (referred to as inward facing state in physiological conditions) to a "closed" state (outward facing state respectively) with a tight contact between the NBDs and where the substrate is released. Upon ATP hydrolysis, the protein switches back to its open state and its V-shape. The extent of the conformational change depends on the ABC transporter, but the gap between NBDs can be as large as a few nanometers[16] (Supplementary Fig. S1A and S1B).

In this study, based on its large conformational changes, we have selected BmrA, a homodimeric multi-drug resistance exporter from *B. subtillis*, to study the effect of membrane curvature on its function and conformational dynamics. The structure of BmrA is known in the closed form[19], highly similar to the closed conformation of other bacterial exporters, with NBDs in close contact. We had previously reconstituted Apo BmrA in vesicles at high density and determined a low resolution cryo-EM structure, showing that NBDs were separated by a few nanometers and a conicity of 15-20° ($\pi/12$-$\pi/9$) in the apo conformation[20], very similar to the conicity of the analog MsbA reconstituted in nanodiscs (Supplementary Fig. S1C). We also revealed a major morphological remodeling of the membrane, from curved to planar, between BmrA reconstituted in apo and closed form in high protein density, respectively[21]. This demonstrates BmrA's ability to bend the membrane depending on its state. A very recent cryo-EM structure of BmrA in detergent confirmed that the apo conformation is indeed open

with dissociated NBDs, 2.6 nm away with respect to the closed form and a conicity of 28° (π/7) (Supplementary Fig. S1C)[22]. Altogether, we expect that substantial conformational changes of individual BmrA within the membrane will lead to local membrane deformations, dependent on its conicity during its ATP cycle. Conversely, the conformational changes and function of BmrA should be modulated by membrane curvature.

Practically, snapshots of ABCs' conformations have been derived with structural techniques (X-Ray, NMR and more recently cryo-EM)[16,23]. Moreover, dynamical conformational changes have been detected on different ABCs, such as the bacterial BmrCD[24], MsbA[25] and McjD[26] or the human Pgp[27,28] and MRP1[29] with DEER, LRET or smFRET. Most of these studies were performed on proteins solubilized in detergent micelles or embedded in ~ 10 nm lipid nanodiscs, where the effect of membrane curvature cannot be addressed. Here, we have reconstituted BmrA in Small Unilamellar Vesicles (SUVs) of various diameters in low protein density. First, we have measured a reduction of ATPase activity for the smallest liposomes. Next, after fluorescent labeling of BmrA on specific NBD residues where the distance is the largest in the apo form, we used TIRF microscopy on immobilized liposomes to detect conformational changes with smFRET. We observed an open (apo) conformation, and a closed one in the presence of ATP or of a non-hydrolysable ATP (AMP-PNP). Interestingly, the fraction of proteins in closed conformation decreases in both cases with increasing membrane curvature, consistent with the observed decrease in activity. Moreover, we propose a theoretical model based on membrane mechanics to quantitatively predict the role of membrane shape and elasticity in the control of the ATPase activity of ABC transporters.

Results

BmrA ATPase activity decreases with increasing membrane curvature

We first purified BmrA in detergent (N-dodecyl-β-D-maltoside (DDM)) and measured an ATP hydrolysis rate of 0.17 µmol/ATP/mg/min at 37°C. Next, using a standard procedure, we reconstituted the proteins in small unilamellar vesicles (SUVs) made of 90% (w/w) Egg Phosphatidyl Choline (EPC) doped with 10% of brain Phosphatidyl Serine (bPS), a negatively charged lipid known to stimulate the ATPase activity of some ABC transporters[30]. BmrA (with a molecular weight M = 130 kDa for the homodimer) was incorporated at 1:13000 molar (homodimer) Protein Lipid Ratio (PLR) (see Materials & Methods for detailed protocols). We found that by adjusting the SUVs preparation temperature, we could obtain two different size distributions of the proteoliposomes, which we characterized by cryo-EM (Fig. 1B): i) upon preparation at 20°C, a broad distribution of large vesicles "LV", with a diameter ø = 123 ± 41 nm; ii) upon reconstitution at 4°C, a narrow distribution of very small vesicles "SV", with a diameter ø = 29 ± 6 nm, implying that these SVs contain one homodimer, in average. Importantly, the conformation of the reconstituted protein, in apo form or in the presence of ortho-vanadate (Vi) (a commonly used inhibitor that prevents from the NBDs dissociation) had no impact on the size of the small liposomes (ø = 29 ± 6 nm with Apo BmrA and ø = 30.0 ± 6 nm for ATP Vi BmrA). Moreover, these cryo-electron microscopy images showed that liposomes were unilamellar without multilamellar vesicles (Fig. 1B).

With floatation in sucrose gradient, we measured 90-95 % protein incorporation in both samples (middle and top fractions) without aggregated proteins in the bottom fraction (Fig. 1C). Finally, by cleaving the NBD with trypsin, we showed that for LV and SV respectively, 85% and 75 % of the proteins had their NBDs facing outside the liposomes, respectively, thus accessible upon addition of ATP in the external medium (detailed protocol in Materials & Methods, Fig. 1D). Thus, proteoliposomes were similar in lamellarity, amount and orientation of incorporated proteins and differed only by their size.

Using a standard enzymatic assay (see Materials & Methods), we measured the ATPase activity A of BmrA for these two populations of liposomes, at PLR=1:13000 molar, in the presence of a saturating concentration of ATP (5 mM). We found that BmrA activity strongly decreased when reducing the liposome size. Indeed, at 37°C, we measured a 2.9-fold lower activity in the highly curved liposomes SV (A=1.7 µmol ATP/min/mg of protein), as compared to the larger vesicles LV (A = 5 µmol ATP/min/mg of protein) (Fig. 1E); this corresponds to a turnover τ = 543 ms in SV and τ = 185 ms in LV for the hydrolysis of one ATP molecule per BmrA molecule, respectively ($\tau = 60.10^3/A \times M$, in seconds, with M the protein molecular weight). The activity is comparable to previously published data on liposomes containing BmrA (~6 µmol of ATP/min/mg)[31] or the closely-related ABC transporter MsbA (~5 µmol of ATP/min/mg)[32]. Note, we performed our experiments without a substrate as BmrA activity is weakly dependent in its presence[18,31]. Our data showed that membrane curvature strongly impacts BmrA activity; however, the protein is able to maintain its cycle in spite of the mechanical stress experienced in the context of the small liposomes. To further decipher the consequences of this strain on the protein conformational changes, we have next investigated the effect of membrane curvature on BmrA structure using single molecule FRET.

Single-molecule FRET assay to monitor the conformational dynamics of BmrA in LV and SV liposomes

In order to fluorescently label the homodimeric BmrA for smFRET experiments (Fig. 2A), we used the two native cysteines C436 located at the basis of the NBDs, close to the TMDs, for which the distance change during the protein cycle, thus the FRET change, are expected to be the largest (Supplementary Fig. S1A and S1B). Among other FRET pairs that we have tested, sulfo-Cy3/sulfo-Cy5 happened to be the most suitable in terms of photochemistry, labelling ratio, and protein activity preservation (Materials & Methods; Supplementary Fig. S2). The activity of the labelled proteins was conserved at 80% as compared to the non-labelled protein. Moreover, due to the homodimeric nature of BmrA, only 24% of the proteins carry both fluorophores.

Our FRET experiments were performed using TIRF microscopy with alternating laser excitation (ALEX) at 532 nm (Donor = sCy3) and 638 nm (Acceptor = sCy5)[33]. We measured the intensities I_D, I_F and I_A of single molecules versus time in the Donor, FRET and Acceptor channels, respectively, with an acquisition rate of 1/200 ms^{-1}. Upon following selection criteria (described in Materials & Methods), we retained data points corresponding to molecules labelled with both a donor and an acceptor, for which we measured over time the apparent uncorrected FRET efficiency $E_{app} = \frac{I_F}{(I_F+I_D)}$ until either the donor or the acceptor bleaches (an oxygen scavenger solution was used to limit bleaching). We then plotted the distribution of instantaneous E_{app} values from multiple traces (total number of proteins N_{prot} > 100), and performed a single or double Gaussian fit, extracting a peak mean position $<E_{app}>$ and a width parameter w (equation and parameters are defined in Material & Methods). The sensitivity of our system was checked with a well-established assay[34,35] (Supplementary Information; Supplementary Fig. S3; Supplementary Table S1), using three 40 base-pair double-stranded (ds) DNAs, carrying the same donor/acceptor pair, at distances ranging between 3 and 7 nm, similar to interdye distances on BmrA and its homologs (Supplementary Fig. S1A and S1B).

We have next implemented a parallelized FRET assay where the conformation of single proteins embedded in multiple liposomes immobilized on a glass substrate can be followed over time (protocol adapted from [36]). The liposomes, containing 0.5% of biotin-PEG-DSPE, were immobilized onto custom-made flow cells, extensively cleaned to get rid of fluorescent contamination (Supplementary Fig. S4A) and pre-treated with silane-PEG-biotin and neutravidin (Fig. 2A). Typical microscopy images of Donor and FRET channels are depicted on Fig. 2B. The specificity of this tethering strategy was

167 confirmed since very few liposomes are bound to the surface in the absence of neutravidin
168 (Supplementary Fig. S4B). Single molecule experiments require to have maximum one protein
169 (homodimer) per liposomes. In practice, we aim for having about one tenth of liposomes containing a
170 protein, reducing the probability to have two proteins per liposome to 1%. To determine the
171 concentration of protein required to be in this regime, we have incorporated sCy5-labelled BmrA in
172 fluorescently labelled SV liposomes with 0.01% of BODIPY®-FL-C5-HPC lipid, which allowed
173 detecting simultaneously the liposomes and the proteins (Fig. 2C). For PLR= 1:81200, we found that
174 40% of vesicles co-localized with sCy5-BmrA while 60% did not contain any protein. For PLR=
175 1:406000, only 5% of the liposomes contained a protein. We have thus reconstituted the transporter at
176 PLR= 1:326000 in the SV, and PLR= 1:650000 in the LV. Finally, we established that the bound
177 vesicles remained sealed and non-permeable to small molecules by encapsulating the soluble dye
178 pyranine in the liposomes labelled with 0,5% of Texas Red® DHPE (Fig. 2D). Co-localization of both
179 fluorescent signals indicated that up to 80% of liposomes were intact after tethering to the surface. We
180 found that the percentage of intact liposomes decreased when increasing the PEG-Biotin density on the
181 surface, due to membrane ripping open. We selected a PEG-Biotin density of 1% for our experiments.
182 Finally, we noted that the average fluorescence lifetime of the dyes was much shorter when linked to
183 BmrA than to the DNA molecules (Supplementary Informations; Supplementary Fig. S3), on average
184 7 seconds for labelled-BmrA while DNA could be observed up to several minutes, even in the presence
185 of the same oxygen scavenger system (Materials and Methods). This effect could be due to an enhanced
186 photostabilization of the cyanines dyes upon interaction with the DNA bases[37].

187 **BmrA exhibits two conformations upon addition of ATP analogs**

188 It is largely reported that type IV ABC exporters switch between two extreme states during the transport
189 cycle: i) a nucleotide-free apo-form where the NBDs are separated by a distance that depends on the
190 ABC and ii) a closed form with dimerized NBDs upon nucleotide binding (e.g. ATP)[14]. The lifetime of
191 the closed conformation can be significantly increased by using ATP analogs in the presence of Mg^{2+}.
192 Two commonly used ones are AMP-PNP and ortho-vanadate (Vi)[38]. AMP-PNP is a non-hydrolysable
193 form of ATP, which binds to the NBDs and leads to their dimerization with the protein in a pre-
194 hydrolytic conformation. This binding is reversible, but since it does not involve ATP hydrolysis, the
195 NBDs remain dimerized for a longer time than with ATP. In contrast, in the presence of ATP, ortho-
196 vanadate is expected to form covalent bonds with the ADP phosphate group bound to the NBD,
197 preventing it from being released and therefore maintaining the protein in a closed post-hydrolytic form
198 and inhibiting its ATPase activity. We first confirmed the effect of both compounds on BmrA in 0.05%
199 detergent Anapoe® X-100: BmrA activity (reference value in detergent at 1.5 mM of ATP is A = 2.5
200 µmol of ATP/min/mg and τ = 0.37 s) is strongly reduced by 80 % upon addition of 2 mM Vanadate in
201 the presence of 1.5 mM of ATP (ATP-Vi) (A = 0.52 and τ = 1.8 s), and by only 30% while adding 5
202 mM AMP-PNP (A = 1.82 and τ = 0.5 s) (Supplementary Fig. S5).

203 We have then used our single-molecule assay to measure the FRET efficiency and thus the
204 conformations of single BmrA molecules in the presence of ATP-Vi or AMP-PNP in the SV and LV
205 liposomes. In both cases, the analogs were added *prior to reconstitution* at a concentration of 5 mM to
206 the mix of protein/lipid in detergent. In order to work at constant nucleotide concentration and reduce
207 dissociation due to nucleotide depletion, the analogs were kept at 5mM in the observation buffer during
208 the smFRET experiments.

209 In the presence of Vi that inhibits BmrA activity by 80% in detergent, we expected to observe mainly
210 a high FRET conformation, corresponding to the closed state of the dimer. Surprisingly, the FRET
211 efficiency histograms exhibited a two-peak distribution in both LV and SV populations (Fig. 3A; 2D

212 histograms with apparent efficiency E_{app} and stoichiometry S_{app} are available on Supplementary Fig.
213 S6; Table 1). This demonstrates the co-existence of two states: i) a high FRET peak at $<E_{app}> = 0.45$,
214 corresponding to the closed state with an interdye distance of about 4 nm from known structures[19]
215 (Supplementary Fig. S1); ii) a low FRET $<E_{app}> = 0.10$, corresponding to an open conformation where
216 the NBDs are separated about 7 nm according to the recent structure[22]. From the two-Gaussian fit, we
217 extracted the respective weight of the low and high-FRET populations; we found that they have the
218 same weight for both LV and SV, around 50% (Table 2). Importantly, no transition was detected
219 between the open and closed state on individual time traces (Fig. 3C-D). This result is also enforced by
220 measuring the time average FRET efficiency per protein (Supplementary Fig. S7): the histograms
221 present the same low and high-FRET populations. Altogether, this shows that half of the proteins are
222 open, and half are closed during the time of our experiments, independent of the size of the liposomes.
223 Note that, although surprising, such a co-existence of open and closed conformation in ATP-Vi has
224 previously been reported, in nanodiscs and detergent, for BmrA in ensemble experiments[39], for its
225 bacterial homolog MsbA[25], human homolog Pgp[28], and for the heterodimer BmrCD[24], without any
226 further explanation.

227 For proteins reconstituted in the presence of 5 mM AMP-PNP, we also observed a bimodal distribution
228 with peaks at similar positions as in the presence of ATP-Vi, showing the co-existence of the same open
229 and closed states: one at low FRET ($<E_{app}> = 0.15$ for the LV and $<E_{app}> = 0.16$ for the SV) and one at
230 high FRET ($<E_{app}> = 0.47$ for the LV and $<E_{app}> = 0.43$ for the SV) with no switch between these
231 conformations (Fig. 3B; Table 1; Supplementary Fig. S6 and S7). However, the relative fractions of
232 these states are different from the ATP-Vi condition. First, the fraction in the closed state P_{cl} is lower
233 in AMP-PNP (32% in LV and 21% in SV) (Table 2) than in presence of ATP-Vi (50%), in line with
234 our activity measurements in detergent showing a stronger inhibition by ATP-Vi. Similar differences
235 between these analogs were reported on human ABC Pgp[28,40] or ABCB7[41]. Second, in contrast with the
236 ATP-Vi, the fraction in a closed state is reduced by about 30% in the smallest liposomes SV as
237 compared to the population with a larger size. Altogether, this suggests that, in the presence of AMP-
238 PNP, the NBDs dimerization rate depends on membrane curvature.

239 **The fraction of BmrA in closed conformation decreases with membrane curvature**

240 We then investigated the conformational changes of BmrA during its ATPase cycle. We first assessed
241 the apo-BmrA conformation (in the absence of ATP) when reconstituted in LV and SV liposomes (Fig
242 4A-B top histograms; Supplementary Fig. S6). As expected, we observe a peak at low FRET for both
243 vesicle sizes. Although these distributions would be fitted with a single Gaussian (Supplementary Fig.
244 S8), a better fit was obtained (notably for SV) with a double Gaussian while fixing the position of a
245 second peak at 0.45, as measured above with the ATP analogs. In this case, we found that a large
246 majority of proteins (92 % for the LV and 86% for the SV (Table 2)) are in the open conformation. The
247 low FRET peak is centered at $<E_{app}> = 0.11$ for the LV and $<E_{app}> = 0.14$ for the SV (Table 1), similar
248 to the low-FRET state observed under addition of ATP analogs. This demonstrates that apo-BmrA
249 exhibits a wide-open conformation in vesicles, independent of membrane curvature.

250 We finally studied the effect of ATP on the conformational distribution. Interestingly, upon addition of
251 5mM Mg-ATP, we observed differences between the two vesicle populations (Fig. 4A-B bottom
252 histograms; Supplementary Fig. S6). As above, we analyzed the FRET distributions with a double
253 Gaussian and by setting the high-FRET peak at 0.45 (parameters in Table 1). We found that the position
254 of the peak corresponding to the open form remains essentially unchanged, 0.13 for the LV and 0.12
255 for the SV. However, as compared to the apo condition, we detected a second high-FRET population
256 corresponding to the closed form, with a fraction P_{cl} that depends on the SUV size. Addition of ATP

resulted in an increase of 13,1% of closed protein population compared to the apo form for the LV, but only in 4,1% for the SV (Fig. 4C; Table 2). Though a rare observation, we detected a switch between both conformations on some traces (examples are in given in Supplementary Fig. S9, where ATP-induced conformational dynamics is visible): 2 times over 226 proteins for the LV and 3 times over 130 proteins for the SV. Despite the oxygen scavenger present in our buffer, the traces recording lasted 7 seconds on average before bleaching. This indicates, for most of the single proteins we have considered, that they are either open or closed for a few seconds. Globally, these data confirm our measurements at the ensemble level that BmrA activity and thus its conformational changes depend on membrane curvature.

Modeling the effect of membrane curvature on the open to close transition probability

We then have developed a model to quantify the influence of membrane mechanics on the cycle of conformational change of BmrA. In order to simplify the theoretical description, we assume that the change of protein conformation can be described by a single reaction coordinate, the V shape angle θ (Fig. 4D). In the absence of nucleotide, the protein energy landscape $E_p(\theta)$ is assumed to have a minimum in the open (apo) conformation θ_{op}, which we model for simplicity as a quadratic energy with a stiffness A: $E_p(\theta) = A\left(\theta - \theta_{op}\right)^2$ (Fig. 4E). Thermal fluctuations can bring the protein to its closed conformation θ_{cl}, and if nucleotides are bound to the two NBDs, the landscape gains a deep minimum at θ_{cl} characterized by a binding energy ε when the NBDs bind to one another. We may consider two types of nucleotides, ATP or the non-hydrolysable AMP-PNP. With ATP, the binding energy is assumed to be so large that the protein remains in the closed conformation until ATP hydrolyses, which occurs at a prescribed rate k_{ATP}. With AMP-PNP, the system is considered to be at thermodynamic equilibrium and the closed-open transition occurs when thermal fluctuations bring the protein over the energy barrier ε. Membrane mechanics modify the transition rates through the energy of membrane deformation associated to the protein shape changes. This term depends on the membrane's bending rigidity and on the geometry of the liposome in which the protein is embedded (Supplementary Fig. S10). Membrane shape optimization can be performed analytically under the assumption of small deviations from a spherical shape (all details of the model are provided in Supplementary Information). Under this condition, we find that the membrane energy scales as $E_m(\theta) = 2\pi\kappa\left(\frac{a}{R}\right)^2(\theta - \theta_R)^2$, where κ is the membrane's bending rigidity, a and R are the protein and SUV radii, and the optimal opening angle is $\theta_R = sin^{-1}(a/R) \approx a/R$ if the SUV is in the optimal state and have a spontaneous curvature $2/R$.

In the thermal equilibrium case, the probability ratio of open P_{op} and closed conformation P_{cl} follows a Boltzmann statistic. In the non-equilibrium case (when ATP is hydrolyzed), this ratio has a steady-state value given by the balance between the thermal flux (from the open to the closed conformation) and the active reversed flux. Writing $\Delta E_i = E_i(\theta_{cl}) - E_i\left(\theta_{op}\right)$, we find:

$$\textit{Equilibrium: } \frac{P_{op}}{P_{cl}} = e^{\left(\Delta E_p + \Delta E_m(R) - \varepsilon\right)/kT} \;\mid\; \textit{Non-equilibrium: } \frac{P_{op}}{P_{cl}} = \frac{k_{ATP}}{k_0} e^{\left(\Delta E_p + \Delta E_m(R)\right)/kT} \qquad (1)$$

where kT is the thermal energy and k_0 is a typical rate of thermal fluctuation of the protein conformation. In the non-equilibrium case, one can also derive the rate of ATP hydrolysis per protein $1/\tau$ as:

$$\frac{1}{k_0\tau} = \frac{k_{ATP}/k_0}{1 + (k_{ATP}/k_0)e^{\left(\Delta E_p + \Delta E_m(R)\right)/kT}} \qquad (2)$$

Through the energy difference $\Delta E_m(R) = 2\pi\kappa\left(\frac{a}{R}\right)^2\left(\theta_{op}-\theta_{cl}\right)\left(2\frac{a}{R}-\theta_{cl}-\theta_{op}\right)$, Eqs.(1,2) provide the size-dependence of the open and closed populations, as well as the rate of ATP hydrolysis. As the open conformation is facing outward, we expect $\theta_{op} > 0$ and $\theta_{cl} < 0$ and $\Delta E_m > 0$ for liposomes with large curvature (Supplementary Fig. S1C). Therefore, we expect the closed conformation to be disfavored, and the rate of ATP hydrolysis to be lower for the smaller SUVs (SV) compared to the larger ones (LV). Note that a proper description of the experimental observation must account for the fact that each sample contains a distribution of vesicle size.

One important prediction of the model is that the open-to-close probability ratio for the two distributions of vesicle size are related by a Boltzmann factor that only involves the membrane deformation energy ($e^{\left(\Delta E_m(V20)-\Delta E_m(V125)\right)/kT}$) both in the equilibrium (AMP-PNP) and non-equilibrium (ATP) case. This prediction agrees with our observations (Fig. 4F, top; Supplementary Fig. S11A), with $\Delta E_m(SV) - \Delta E_m(LV) \simeq (0.7 \pm 0.2)kT$. Based on BmrA and homologs' structures, we used a protein diameter $2a \approx 4nm$ (Supplementary Fig. S1D). Since the conicity of the closed conformation is independent of the protein membrane environment[25,28], θ_{cl} was set to $-\pi/10$ measured from closed BmrA structure in detergent (Supplementary Fig. S1C). Conversely, it was reported that the opening of the apo form of homologs MsbA and Pgp changes between detergent and nanodisc environments[25,28]. Therefore, we used $\theta_{op} \approx +\pi/10$, corresponding to MsbA structure in membrane (nanodisc), in good agreement with the angle measured for BmrA in vesicles at high protein density but low resolution[20] (Supplementary Fig.S1A and S1C). Fitting our data with these parameters leads to a membrane bending rigidity $\kappa \approx (21 \pm 5)kT$, which is in line with expected values[42]. Note that $\Delta E_m/kT$ is very small for large SUVs ($\simeq 6 \cdot 10^{-3}$) so that proteins are not sensitive to membrane elasticity, while the open-to-closed transition should be moderately impaired in the smaller SUVs ($\Delta E_m/kT \simeq 0.7kT$), as observed. Knowing the membrane parameters from the previous fit, we can determine the value of the relevant combination of protein parameters in the active case for the chosen ATP concentration: $(k_{ATP}/k_0) \cdot e^{\Delta E_p/kT} \simeq 5$. This lets us predict how the protein activity (the rate of ATP hydrolysis) depends on the liposome size (Fig. 4F, bottom; Supplementary Fig. S11B). In the case of our experiments, we predict that it is reduced by about 50% for the small SUVs as compared to the larger ones, a value in very good agreement with the experimental value obtained from ensemble measurements (Fig. 4F, bottom).

Discussion

In general, mechanosensitive membrane proteins have been identified through the cell response after mechanical stresses and then, the corresponding molecular mechanism linked to their function studied at the structural level. Previous studies on MsbA[43] and on ABC importers OpuA[44] and ButCD[45] have highlighted the effect of the local environment for ABC transporters, showing at the single-molecule level different degrees of opening of the apo conformation when incorporated in detergent or in lipid nanodiscs. Our smFRET study reveals for the first time that membrane curvature also impacts the conformation of an ABC transporter, as well as its activity. Our experiments, in which we control the curvature of liposomes, demonstrate that the activity of BmrA decreases when increasing membrane curvature, as well as the fraction of proteins in a closed conformation. These results can be recapitulated with a theoretical model based on the idea that the protein conformation changes are associated to membrane deformation and are therefore sensitive to membrane mechanics. As in our experiments, the curvature of the liposome membrane fits the outward facing open conformation better than the closed conformation, membrane energy favors the open state. In bcell, the open conformation is inward facing (toward the cytoplasm), so that the effect of membrane energy should be opposite. It should favor the transition from open to closed conformation and increase the protein's activity. We expect this effect to

be relatively small for BmrA owing to the small value of the product of the cell curvature times the protein size.

Regarding the open conformation, a wide range of openings have been reported among ABC exporters, with NBDs in close contact up to NBD separated by about 6-7 nm[14,16,23,46]. Our smFRET data in vesicles are consistent with the recent 3D model of BmrA in detergent[22] with dissociated NBDs in the apo form. Furthermore, we have shown that the opening of the apo form is independent of the liposome curvature (since the low FRET value does not change between LV and SV), in contrast with the transition rate between both conformations. Former studies on bacterial MsbA and human PgP stressed that this relative opening is wider in detergent than in lipid nanodisc[25,28], suggesting that the protein environment influences the structure of these transporters. In our model, using the open angle $\theta_{op} \approx +\pi/7$, deduced from the BmrA structure in detergent (Supplementary Fig. S1C), led to a membrane bending rigidity $\kappa \approx (29 \pm 7)kT$, when fitting to the population and activity curves. For the full range of liposome size we explored, θ_{op} is larger than the optimal opening angle fixed by the vesicle size θ_R, so that the energy difference ΔE_m decreases with θ_{op} in this regime (see Eq. 11, SI theory), hence a higher fitted value of κ.

Our activity measurements have highlighted that the turn-over of ATP-hydrolysis increases from 0.18 s to 0.54 s between the LV and SV liposomes. In principle, by monitoring smFRET over a few seconds, we anticipated to detect conformational dynamics, which was not the case. Experimentally, activity was measured at 37°C, while smFRET experiments were performed at room temperature in order to limit evaporation in the small observation volumes used. In these conditions, a reduction of activity by only a factor about 4 was expected, based on previous measurements on Pgp[47]. In fact, for BmrA, with our ATPase assay, we found out that its activity is reduced by a factor 20 over this temperature range (Supplementary Fig. S12). Hence, this explains the slow turn-over in our smFRET experiments and the low probability of detecting conformational transitions. Nevertheless, by measuring the average lifetime of the proteins in the high-FRET state in LV (with $E_{avg} > 0.3$, N = 38 proteins /226), we can conclude that in these conditions and at 20°C, the lifetime of the closed state is longer than 7 seconds. This value is of the same order of magnitude than the average turnover measured in cuvette for the LV and SV (respectively 3.7 and 7 seconds). Similarly, at room temperature, lifetime of a few seconds was found for the closed state of McjD[26] and more recently of the human ABC CFTR[48].

Our model predicts that such an effect of membrane curvature can be expected for all type-IV ABC exporters, provided that the apo form is sufficiently open, since they have similar size and well-conserved closed conformations. From the model, we infer that ABCs with BmrA characteristics are mechanosensitive only at large membrane curvature, higher than 0.08 nm^{-1} (i.e. for liposomes smaller than 40 nm diameter), and that this property is negligible in vesicles with diameter bigger than 70 nm. The human Pgp being a close homolog to BmrA (Supplementary Fig. S1), we expect that membrane bending should not affect its function in usual transport vesicles inside cells, or endosomal compartments. Nevertheless, significant effects should be detected at weaker curvature for proteins with a larger membrane imprint (a) and/or with higher conicity (θ_{op} and θ_{cl}) (Supplementary Fig. S13). Membrane bending rigidity (κ) can also modulate the conformational switch (Eq. (2)). Consequently, changing membrane stiffness by adjusting lipid composition (e.g. via cholesterol or sphingomyelin concentration) is expected to tune the sensitivity of the activity to membrane curvature.

Altogether our results demonstrate that membrane curvature plays a role in the transport cycle kinetics of ABC transporters. This invites us to re-think the definition of *mechanosensitivity* to also include other proteins whose activity involves large shape changes within the membrane. BmrA's sensitivity to membrane bending suggests a potential response to membrane tension. However, curvature and

387 membrane tension could have different consequences. While the effect of membrane tension on
388 mechanosensitive proteins has been largely documented, it would be worth to investigate the effect of
389 tension on the function of this new class of mechanosensors.

390 **Materials and Methods**

391 **Reagents**

392 Egg Phosphatidylcholine (EPC), brain Phosphatidylserine (bPS), 1,2-distearoyl-sn-glycero-3-
393 phosphoethanolamine-N-[biotinyl(polyethylene glycol)-2000] (DSPE-PEG(2000)-Biotin) and 1,2-
394 dihexadecanoyl-sn-glycero-3-phosphoethanolamine, triethylammonium salt (Texas Red® DHPE) were
395 from Avanti Polar Lipids (Alabaster, AL, USA). All lipids were purchased in CHCl3 stock solution.
396 BODIPY®-FL-C5-HPC was purchased from Invitrogen. N-dodecyl-β-D-maltoside (DDM) and
397 Anapoe® X-100 (Triton® X-100) were purchased from Anatrace (Maumee, OH, USA). 50 mesh
398 BioBeads® were purchased from Bio-Rad (Hercules, CA, USA) and prepared according to [49]. Lacey
399 carbon electron microscopy grids were purchased from Ted Pella (Reding, CA, USA). Nucleotides,
400 ATP, AMP-PNP, ATPase inhibitor orthovanadate, pyranine and all other chemicals were purchased
401 from Sigma Aldrich (Merck KGaA, Darmstadt, Germany). SulfoCy3 and SulfoCy5 maleimide probes
402 were purchased from Lumiprobe GmbH (Germany). Coverslips for the custom-built chambers were
403 purchased from Menzel-Gläser (Germany) (thickness #1). Silane-PEG2000 and silane-PEG3400-biotin
404 were purchased in powder from LaysanBio (Alabama, USA) and dissolved in DMSO. Neutravidin and
405 (from bovine milk > 98%) were purchased from Sigma Aldrich (Merck KGaA, Darmstadt, Germany).
406 Double stranded DNA for FRET calibration was purchased from Eurofins Genomics (Ebersberg,
407 Germany). D-glucose, glucose oxidase and Trolox were purchased from Sigma Aldrich. Catalase from
408 bovine liver was purchased from MP Biomedicals (California, USA).

409 **BmrA expression, purification and labelling**

410 His-C-ter-BmrA was expressed in *E. coli* and purified in 0.05 % DDM as previously reported[20]. Elution
411 buffer from Ni-NTA agarose beads was 50 mM Tris, pH 8.0, 100 mM NaCl, 250 mM imidazole, pH
412 8.0, 10% glycerol, 0.05% DDM. Proteins were eluted at 0.3-1.5 mg/mL and used without further
413 concentration as it caused protein aggregation (observed in EM). Purified proteins were aliquoted in 50
414 µL volume and kept at -80°C before use. Aliquots were thawed only one time before experiments.
415 Protein concentration was measured by Bradford method.

416 For smFRET experiments, purified BmrA collected from elution step was fluorescently labelled using
417 maleimide dyes on C436, the sole Cys residue, and thus two C436 were labeled per homodimer of
418 BmrA. Several couples of donor/acceptor dyes were evaluated according to the rate of labelling and the
419 ATPase activity of the labelled proteins including Alexa488/Atto610, Alexa488/sulfoCy5,
420 Cy3B/sulfoCy5 and sulfoCy3/sulfoCy5 selected based on spectrum overlap, dye photostability and
421 published data. Best results have been obtained with sulfoCy3/sulfoCy5. BmrA in detergent was
422 incubated with sulfo-Cy3 and sulfo-Cy5 maleimide dyes, at sCy3/sCy5/protein 10/10/1 mol/mol/mol,
423 overnight at 4°C (Supplementary Fig. S2). Thiol-maleimide reaction was performed at pH 7. Unbound
424 dyes were removed by binding BmrA at pH 8 on Ni-NTA agarose beads in batch followed by washing
425 with 5 volumes of a free dye buffer before elution with 250 mM imidazole. Labeled BmrA was analyzed
426 on SDS-PAGE gel by fluorescence and stained with Coomassie blue. Several populations were present
427 after labeling: BmrA without labeling, donor only, acceptor only, dual-labeled (donor-acceptor),
428 donor/donor and acceptor/acceptor. The rate of labelling was calculated from the concentration of
429 fluorescent dyes measured by absorbance sCy3 (molar extinction coefficient ε_{max} = 162 000 $cm^{-1}.M^{-1}$),

430 sCy5 (ε_{max} = 281 000 $cm^{-1}.M^{-1}$) and protein concentration by Bradford assay. ATPase activity was
431 measured as described below and sCy3/sCy5 labelled BmrA retained 80% of the unlabeled protein.

432 **Reconstitution of BmrA in proteoliposomes**

433 Proteoliposomes containing BmrA were formed by detergent removal using Bio-Beads® from a fully
434 solubilized mixtures of lipid/protein/detergent, as reported previously[31] and according to the principle
435 reviewed in [50,51]. We first prepared pure lipid liposomes composed of EPC:bPS 90:10 w:w,
436 supplemented with 0.5% of biotin-PEG2000-DSPE to allow liposomes immobilization for the smFRET
437 study. A dried lipid film was obtained by evaporating organic solvents from the lipid mix. Lipids were
438 then resuspended in water at 10 mg/mL, sonicated with a tip sonicator for one minute while keeping
439 the solution on ice. 50 µL aliquots were made and samples were kept frozen at -20°C. For each
440 reconstitution, an aliquot of lipid vesicles was resuspended at 2 mg/mL in 50 mM MOPS, 150 mM
441 NaCl, 1 mM $MgCl_2$, pH 7.5, then lipids were solubilized with Anapoe® X-100 for 15 minutes at
442 detergent/lipid ratio of 2.5 w:w. It is worth noting that BrmA is stable and functionally active both in
443 Anapoe® X-100 and in DDM, allowing the use of different detergents for lipid solubilization and
444 purification of BmrA. After lipid solubilization, BmrA was added at a protein to lipid ratio (PLR) of
445 1:650000 for LV and 1:325000 for SV. This PLR ensured that less than one BmrA homodimer was
446 incorporated per proteoliposome. Inhibition of the protein was performed upon addition of 2 mM
447 orthovanadate (Vi) and 5 mM ATP, or of 5 mM AMP-PNP, in the presence of 5 mM MgCl2 in the
448 buffers. The solution was incubated for 15 minutes, then detergent removed by the addition of
449 BioBeads® under gentle stirring. Detergent removal was performed at 20°C and 4°C respectively to
450 produce the LV and SV populations. The BioBeads® were added in three rounds at the following
451 BioBeads®/ Anapoe® X-100 ratio: i) for the LV population, 10 w:w for 2h, then 10 w:w for 1h and 20
452 w:w for 1h; ii) for the SV population, 30 w:w for 2h, then 30 w:w for 1h and 60 w:w for 1h. Note that
453 the amount of BioBeads® was increased during the reconstitution at 4°C (SV) to ensure that the rate of
454 detergent removal was similar than at room temperature. These amounts of BioBeads® were sufficient
455 to remove all detergent molecules including the amount of DDM present in the preparation of BmrA[52].
456 As also shown previously, at this low PLR, negligible amounts of lipid and no protein were adsorbed
457 onto the BioBeads®[53]. After detergent removal, the reconstituted supernatants were removed and stored
458 for no more than 24h at 4°C before analysis. It is worth noting that ATPase activities were stable for at
459 least 24h at 4°C as proteoliposomes remained unchanged as seen by cryo-EM.

460 **Protein incorporation and orientation in proteoliposomes**

461 Protein incorporation in the population of vesicles was measured after separation of proteoliposomes,
462 aggregated proteins and protein-free liposomes by sedimentation in a sucrose gradient according to a
463 protocol modified for proteoliposomes[54]. BmrA was reconstituted at PLR=1:9750 in EPC-PS 9/1
464 mol/mol and 2 mg/mL lipid concentration at 20°C or 4°C. Floatation assay was performed with
465 polycarbonate centrifugation 11x34 mm tubes (Beckman Coulter, USA) and sucrose solutions prepared
466 in HK buffer, i.e. 50 mM Hepes, pH 7.5, 150 mM NaCl. An aliquot of 150 µL of proteoliposomes was
467 gently mixed with 100 µL of 60 % sucrose solution. Then, 200 µL of a second layer of 24% sucrose
468 was added followed by 100 µL of HK buffer. Tubes were ultracentrifuged 90 minutes in a TLS-55
469 Swing bucket rotor (Beckman) at 55,000 rpm at 4°C with a slow acceleration and deceleration steps
470 (5/5). Fractions were gently pipetted off with a syringe and analyzed by 4-12% NuPage gel after staining
471 with Commassie Blue. Protein intensities and incorporation yield were measured with the Amersham
472 Imager 680 and the analysis Software, version 2.0.0.

473 Protein orientation in the membrane of reconstituted proteoliposomes was determined from gel
474 electrophoresis patterns before and after trypsin treatment of the reconstituted samples[55]. To this end

475 proteoliposomes reconstituted with Alexa-488 labeled BmrA were reconstituted at 20°C or 4°C.
476 Proteoliposomes were incubated at room temperature for 20 minutes in the presence of trypsin
477 (trypsin/protein 1:1 w:w). The reaction was stopped by 2 µL of cOmplete™, EDTA-free Protease
478 Inhibitor Cocktail. Since proteoliposomes were non permeable to trypsin, only proteins with NBDs
479 pointing outward of vesicles were proteolyzed. Control experiments of proteolysis of all proteins was
480 performed on Anapoe® X-100 solubilized proteoliposomes (Anapoe® X-100:lipid 2.5 w:w). Percent
481 of protein orientation was determined from the ratio of the fluorescence intensities of the BmrA
482 monomer band (M~ 65 000) before and after trypsin digestion (Amersham Imager 680 and analysis
483 Software, version 2.0.0).

484 **ATPase activity**

485 ATP hydrolysis was carried out using a coupled enzyme assay of pyruvate kinase, and lactate
486 dehydrogenase by absorbance changes of NADH/NAD+ ratio at 340 nm[31]. All measurements were
487 made in triplicates. ATPase activity was measured in 50 mM MOPS pH 7.5, 150 mM NaCl, 10 mM of
488 $MgCl_2$ with 1X enzyme cocktail and 0.5-1 µg of protein at 37°C in 150 µL total volume. Absorbance
489 of NADH was measured by spectrometer (Cary Win 60 UV – Vis, Agilent Technologies) at 340 nm
490 every 15 s with quartz cuvette (N.105-254-15-40, Hellma Analytics, 3 x 3 mm). Proteoliposomes were
491 incubated for 4 min at desired temperature. ATP was added at 1.5 or 5 mM final concentration and
492 absorbance was recorded for 4 min but the first minute of reaction was ignored for ATPase activity
493 calculation. Since the K_D of ATP for BmrA is 1 mM, this ensured that BmrA hydrolyzed ATP at
494 maximum rate in all conditions[31]. Rate of inhibition was measured after addition of 2 mM of
495 orthovanadate or 5 mM of AMP-PNP. ATPase activity was calculated by quantity of NADH oxidized
496 equivalent to quantity of ATP hydrolyzed, per min and per mg of protein. ATP hydrolysis of BmrA in
497 micelles of detergent was measured with Anapoe® X-100 0.05% in the cuvette. The amount of BmrA
498 per assay was 1 µg for proteoliposomes and 2 µg for BrmA in detergent.

499 **Cryo-electron microscopy and size measurement of proteoliposomes**

500 Holey formvar lacey grids (Ted Pella, USA) were glow discharged for 30 s under vacuum. Then, 4 µL
501 of 1 mg/mL of proteoliposomes were deposited during 30 s on the grid before flash frozen in liquid
502 ethane with an EM-GP plunger (Leica Microsystems, Germany). Images were taken under low dose
503 condition on a Glacios electron microscope (Thermofisher, USA) operating at 200 KV and recorded
504 with a Falcon IVi camera. Diameter of proteoliposomes were measured manually from cryo-EM images
505 from 594, 262 and 249 vesicles reconstituted at 20°C, 4°C with Apo BmrA and 4°C with ATP Vi BmrA.

506 **Proteoliposomes immobilization for smFRET experiment**

507 A small channel of roughly 10 µL was custom-built between two coverslips (Menzel-Gläser, thickness
508 #1): bottom coverslips is 25 mm diameter, and top squared-shaped coverslip is cut to 18×10 mm^2. The
509 glass coverslips were placed on a Teflon carrier in a glass beaker. They were extensively washed under
510 sonication with the following solutions: chloroform for 20 min (chloroform bath was then discarded
511 and we allow slides to dry under the hood for 5 min), water for 5 min, KOH 1 M for 20 min, rinsed
512 three times in water, and a final wash in water for 15 min. The coverslips were dried under a gentle
513 stream of nitrogen and placed for 2 min in an air plasma cleaner. A double-sided tape mask was used
514 to build the observation chamber. The channel was loaded by using a pipette tip on one side and
515 aspirating at the other side with a clean paper towel Kimwipe. In order to specifically tether the
516 proteoliposomes, the chamber was incubated with a solution of silane-PEG with 1% of silane-PEG-
517 biotin at 5 mM for one hour. The chamber was rinsed by injecting 100 µL of buffer: 50 mM MOPS pH
518 7.5, 150 mM NaCl, 1 Mm $MgCl_2$. 40 µL of 20 µg/mL neutravidin was incubated for 5 to 10min. The

surface was then rinsed with 100 µL of buffer. 40 µL of 1 mg/mL β-casein was incubated at least 10 min and then rinsed with 100 µL of buffer. Finally, 40 µL of proteoliposomes solution was injected at concentration 5.10^{-2} mg/mL and 5.10^{-3} mg/mL in lipids respectively for LV and SV. The solution was incubated for 5 to 10 min then rinsed with 100 µL of buffer before imaging.

Microscopy and smFRET assay calibration

Observation was performed on a Nikon TI-Eclipse microscope equipped with a Nikon TIRF arm, a TIRF oil objective ×100 (NA 1.45, Nikon), a DualView system (Photometrics DV2) and an ORCA-Flash4.0 V3 Digital CMOS camera (Hamamatsu). The DualView system was equipped with a dichroic mirror 633 nm (ZT633rdc, Chroma) and the appropriate filters for the FRET couple sCy3/sCy5 (593/40 and 684/24 respectively, Chroma). We used alternating laser excitation (ALEX) at 532 nm (for sCy3 = donor) and 638 nm (for sCy5 = acceptor) (Lasers Oxxius). Acquisition rate was 1/200 ms^{-1}, with an exposure time of 50 ms in each channel with a 50 ms time-lag in between (necessary to overcome delay issues in our system).

The system was thoroughly calibrated by using a 40 base-pair double-stranded (ds) DNA as previously described in [34,35]. One strand is labelled with a biotin on the 3' end and with Cy3 dye on the 5' end. The complementary strand was modified subsequently on three different T-base with a Cy5 dye, resulting in three distances L_{D-A} between the donor and acceptor fluorophores, respectively 19, 12 and 7 base-pairs. The oligonucleotides are hybridized at a final concentration 15 µM in each oligo, in buffer 10 mM Tris-HCl pH 8, 400 mM NaCl, 1 mM EDTA (buffer TE). The solution is brought to 84.6°C for 10 min, then allowed to cool down to RT. Glass coverslips were extensively cleaned and then built together as described in the previous paragraph. A solution of biotinylated BSA at 1 mg/mL is incubated in the chamber for 5 min and rinsed with 100 µL of buffer TE. The surface is coated with neutravidin at 20 µg/mL for 5 min, rinsed with 100 µL of buffer TE, incubated with β-casein at 1 mg/mL for 10 min and rinsed with 100 µL of buffer TE. Just before observation, the DNA sample is loaded at 30 pM for 2 min and rinsed with 100 µL of buffer TE.

All experiments were carried out utilizing an oxygen scavenging system supplemented with 1 mM Trolox as a photostabilization agent[36]. The oxygen scavenger system consists of 4 mg/mL D-glucose, 1 mg/mL glucose oxidase and 0,04 mg/mL catalase. A 10x D-glucose stock solution could be prepared and stored at -20°C for several months, and a 100x "gloxy" solution (mixture of catalase and glucose oxydase) was prepared and stored at 4°C for up to several months. The Trolox 2x stock solution is prepared at approximately 1-2 mM, with pH adjusted to 7.5, filtered at 0,2 µm and stored in the dark at 4°C up to two weeks. Solutions were mixed to a final 1x concentration at the last minute before observation (solution was filtered a last time at 0,2 µm before to load it in the observation chamber). It is worth noting that the oxygen scavenger system was more effective on the DNA sample, allowing us to observe minutes-long intensity traces, compared to the single-BmrA observation, for which the average fluorescence lifetime was 7 sec.

smFRET analysis

Data analysis was performed with the Matlab code iSMS[56,57], which allows to detect positions of Donor and Acceptor, to find matching pairs Donor/Acceptor by aligning the Donor and Acceptor channels and to output intensities I_D, I_F and I_A respectively in the Donor, FRET and Acceptor channels, of single molecules according to time (all intensities are corrected for background). The automatic bleach detection was used but could be manually adjusted if necessary and blinking intervals were set manually. In the software, the data evaluation process was then performed manually on Donor/Acceptor pairs. We discarded events with more than one bleaching step in either donor or acceptor channel, traces

that showed very rapid photobleaching, or interference of strongly fluorescent neighbouring peaks (resulting in highly noisy intensity trace) were also excluded at this point. For each single molecule, the apparent FRET efficiency $E_{app} = (I_F) / (I_D + I_F)$ and the apparent stoichiometry $S_{app} = (I_D + I_F) / (I_D + I_F + I_A)$ were measured until either the donor or the acceptor bleaches, and were accumulated into a normalized histogram, without applying further corrections. Gaussian fits were performed in Matlab *Curve Fitter* tool. The following equation is used for the Gaussian fit on apparent FRET efficiency E_{app}: $a \times e^{-(E_{app} - <E_{app}>)^2/w^2}$ with a the amplitude, $<E_{app}>$ the mean position and w the parameter related to the Gaussian width. When double Gaussian fit was applied, the parameters of the fit were used to measure the probability to find the protein in low FRET state (= P_{op}) or in high FRET state (= P_{cl}). Errors were measured by applying bootstrapping on our data (10 times).

Theory

See theoretical section of the Supplementary Information.

References

1. Yang, X. *et al.* Structure deformation and curvature sensing of PIEZO1 in lipid membranes. *Nature* **604**, 377–383 (2022).

2. Haselwandter, C. A., Guo, Y. R., Fu, Z. & MacKinnon, R. Quantitative prediction and measurement of Piezo's membrane footprint. *Proc. Natl. Acad. Sci. U. S. A.* **119**, (2022).

3. Brohawn, S. G., Su, Z. & MacKinnon, R. Mechanosensitivity is mediated directly by the lipid membrane in TRAAK and TREK1 K+ channels. *Proc. Natl. Acad. Sci. U. S. A.* **111**, 3614–3619 (2014).

4. Cox, C. D., Bavi, N. & Martinac, B. Bacterial Mechanosensors. *Annu. Rev. Physiol.* **80**, 71–93 (2018).

5. Bavi, O. *et al.* Influence of Global and Local Membrane Curvature on Mechanosensitive Ion Channels: A Finite Element Approach. *Membranes (Basel).* **6**, 14 (2016).

6. Turner, M. S. & Sens, P. Gating-by-tilt of mechanically sensitive membrane channels. *Phys. Rev. Lett.* **93**, 118103 (2004).

7. Haselwandter, C. A., Guo, Y. R., Fu, Z. & MacKinnon, R. Elastic properties and shape of the Piezo dome underlying its mechanosensory function. *Proc. Natl. Acad. Sci. U. S. A.* **119**, (2022).

8. Markin, V. S. Lateral organization of membranes and cell shapes. *Biophys. J.* **36**, 1–19 (1981).

9. Corradi, V. *et al.* Lipid-Protein Interactions Are Unique Fingerprints for Membrane Proteins. *ACS Cent. Sci.* **4**, 709–717 (2018).

10. Schmidt, D. & MacKinnon, R. Voltage-dependent K+ channel gating and voltage sensor toxin sensitivity depend on the mechanical state of the lipid membrane. *Proc. Natl. Acad. Sci. U. S. A.* **105**, 19276–19281 (2008).

11. Aimon, S. *et al.* Membrane Shape Modulates Transmembrane Protein Distribution. *Dev. Cell* **28**, 212–218 (2014).

12. Quemeneur, F. *et al.* Shape matters in protein mobility within membranes. *Proc. Natl. Acad. Sci.* **111**, 5083–5087 (2014).

13. Kluge, C., Pöhnl, M. & Böckmann, R. A. Spontaneous local membrane curvature induced by transmembrane proteins. *Biophys. J.* **121**, 671–683 (2022).

14. Locher, K. P. Mechanistic diversity in ATP-binding cassette (ABC) transporters. *Nat. Struct. Mol. Biol.* **23**, 487–93 (2016).

605 15. Vasiliou, V., Vasiliou, K. & Nebert, D. W. Human ATP-binding cassette (ABC) transporter
606 family. *Hum. Genomics* **3**, 281–290 (2009).

607 16. Januliene, D. & Moeller, A. Cryo-EM of ABC transporters: an ice-cold solution to everything?
608 *FEBS Lett.* **594**, 3776–3789 (2020).

609 17. Thomas, C. *et al.* Structural and functional diversity calls for a new classification of ABC
610 transporters. *FEBS Lett.* **594**, 3767–3775 (2020).

611 18. Orelle, C., Schmitt, L. & Jault, J. Waste or die : The price to pay to stay alive. *Trends Microbiol.*
612 **31**, 233–241 (2022).

613 19. Chaptal, V. *et al.* Substrate-bound and substrate-free outward-facing structures of a multidrug
614 ABC exporter. *Sci. Adv.* **8**, 1–11 (2022).

615 20. Fribourg, P. F. *et al.* 3D cryo-electron reconstruction of BmrA, a bacterial multidrug ABC
616 transporter in an inward-facing conformation and in a lipidic environment. *J. Mol. Biol.* **426**,
617 2059–2069 (2014).

618 21. Orelle, C. *et al.* Conformational change induced by ATP binding in the multidrug ATP-binding
619 cassette transporter BmrA. *Biochemistry* **47**, 2404–2412 (2008).

620 22. Di Cesare, M. *et al.* The transport activity of the multidrug ABC transporter BmrA does not
621 require a wide separation of the nucleotide-binding domains. *J. Biol. Chem.* 105546 (2023).
622 doi:10.1016/j.jbc.2023.105546

623 23. Lewinson, O., Orelle, C. & Seeger, M. A. Structures of ABC transporters: handle with care.
624 *FEBS Lett.* **594**, 3799–3814 (2020).

625 24. Tang, Q. *et al.* Asymmetric conformations and lipid interactions shape the ATP-coupled cycle
626 of a heterodimeric ABC transporter. *Nat. Commun.* **14**, (2023).

627 25. Zoghbi, M. E. & Altenberg, G. A. Luminescence resonance energy transfer spectroscopy of
628 ATP-binding cassette proteins. *Biochim. Biophys. Acta - Biomembr.* **1860**, 854–867 (2018).

629 26. Husada, F. *et al.* Conformational dynamics of the ABC transporter McjD seen by single-
630 molecule FRET. *EMBO J.* **37**, e100056 (2018).

631 27. Verhalen, B. *et al.* Energy transduction and alternating access of the mammalian ABC
632 transporter P-glycoprotein. *Nature* **543**, 738–741 (2017).

633 28. Zoghbi, M. E. *et al.* Substrate-induced conformational changes in the nucleotide-binding
634 domains of lipid bilayer-associated P-glycoprotein during ATP hydrolysis. *J. Biol. Chem.* **292**,
635 20412–20424 (2017).

636 29. Wang, L. *et al.* Characterization of the kinetic cycle of an ABC transporter by single-molecule
637 and cryo-EM analyses. *Elife* **9**, 1–20 (2020).

638 30. Mehmood, S. *et al.* Structural and functional basis for lipid synergy on the activity of the
639 antibacterial peptide ABC transporter McjD. *J. Biol. Chem.* **291**, 21656–21668 (2016).

640 31. Steinfels, E. *et al.* Characterization of YvcC (BmrA), a multidrug ABC transporter constitutively
641 expressed in Bacillus subtilis. *Biochemistry* **43**, 7491–7502 (2004).

642 32. Mi, W. *et al.* Structural basis of MsbA-mediated lipopolysaccharide transport. *Nature* **549**, 233–
643 237 (2017).

644 33. Kapanidis, A. N. *et al.* Fluorescence-aided molecule sorting: analysis of structure and
645 interactions by alternating-laser excitation of single molecules. *Proc. Natl. Acad. Sci. U. S. A.*
646 **101**, 8936–41 (2004).

647 34. Deniz, A. A. *et al.* Single-pair fluorescence resonance energy transfer on freely diffusing

648 molecules: observation of Förster distance dependence and subpopulations. *Proc. Natl. Acad.*
649 *Sci. U. S. A.* **96**, 3670–5 (1999).

650 35. Hellenkamp, B. *et al.* Precision and accuracy of single-molecule FRET measurements—a multi-
651 laboratory benchmark study. *Nat. Methods* **15**, 669–676 (2018).

652 36. Selvin, P. R. & Ha, T. *Single-molecule Techniques: A Laboratory Manual*. *CSHL Press* (2008).

653 37. Lee, W., Von Hippel, P. H. & Marcus, A. H. Internally labeled Cy3/Cy5 DNA constructs show
654 greatly enhanced photo-stability in single-molecule FRET experiments. *Nucleic Acids Res.* **42**,
655 5967–5977 (2014).

656 38. Lacabanne, D. *et al.* ATP Analogues for Structural Investigations: Case Studies of a DnaB
657 Helicase and an ABC Transporter. *Molecules* **25**, (2020).

658 39. Javed, W. *et al.* Structural Insights into the Catalytic Cycle of a Bacterial Multidrug ABC Efflux
659 Pump. *J. Mol. Biol.* **434**, (2022).

660 40. Li, M. J., Nath, A. & Atkins, W. M. Differential Coupling of Binding, ATP Hydrolysis, and
661 Transport of Fluorescent Probes with P-Glycoprotein in Lipid Nanodiscs. *Biochemistry* **56**,
662 2506–2517 (2017).

663 41. Yan, Q., Shen, Y. & Yang, X. Cryo-EM structure of AMP-PNP-bound human mitochondrial
664 ATP-binding cassette transporter ABCB7. *J. Struct. Biol.* **214**, (2022).

665 42. Marsh, D. Elastic curvature constants of lipid monolayers and bilayers. *Chem. Phys. Lipids* **144**,
666 146–159 (2006).

667 43. Liu, Y., Liu, Y., He, L., Zhao, Y. & Zhang, X. C. Single-molecule fluorescence studies on the
668 conformational change of the ABC transporter MsbA. *Biophys. Reports* **4**, 153–165 (2018).

669 44. Tassis, K. *et al.* Single-molecule studies of conformational states and dynamics in the ABC
670 importer OpuA. *FEBS Lett.* **595**, 717–734 (2021).

671 45. Yang, M. *et al.* Single-molecule probing of the conformational homogeneity of the ABC
672 transporter BtuCD. *Nat. Chem. Biol.* **14**, 715–722 (2018).

673 46. Moeller, A. *et al.* Distinct Conformational Spectrum of Homologous Multidrug ABC
674 Transporters. *Structure* **23**, 450–460 (2015).

675 47. Ambudkar, S. V., Cardarelli, C. O., Pashinsky, I. & Stein, W. D. Relation between the turnover
676 number for vinblastine transport and for vinblastine-stimulated ATP hydrolysis by human P-
677 glycoprotein. *J. Biol. Chem.* **272**, 21160–21166 (1997).

678 48. Levring, J. *et al.* CFTR function, pathology and pharmacology at single-molecule resolution.
679 *Nature* **616**, 606–614 (2023).

680 49. Rigaud, J.-L. *et al.* Bio-Beads: an efficient strategy for two-dimensional crystallization of
681 membrane proteins. *J. Struct. Biol.* **118**, 226–235 (1997).

682 50. Rigaud, J. L. & Lévy, D. Reconstitution of Membrane Proteins into Liposomes. *Methods*
683 *Enzymol.* **372**, 65–86 (2003).

684 51. Rigaud, J. L., Pitard, B. & Levy, D. Reconstitution of membrane proteins into liposomes:
685 application to energy-transducing membrane proteins. *BBA - Bioenerg.* **1231**, 223–246 (1995).

686 52. Lévy, D., Bluzat, A., Seigneuret, M. & Rigaud, J. L. A systematic study of liposome and
687 proteoliposome reconstitution involving Bio-Bead-mediated Triton X-100 removal. *BBA -*
688 *Biomembr.* **105**, 179–190 (1990).

689 53. Rigaud, J.-L., Lévy, D., G, M. & Lambert, O. Detergent removal by Bio-Beads. Application to
690 membrane protein reconstitution and two-dimensional crystallisation. *Eur J. Biophys.* **27**, 305–

319 (1998).

54. Mesmin, B. *et al.* XA four-step cycle driven by PI(4)P hydrolysis directs sterol/PI(4)P exchange by the ER-Golgi Tether OSBP. *Cell* **155**, 830 (2013).

55. Lévy, D., Guiik, A., Bluzat, A. & Rigaud, J.-L. Reconstitution of the sarcoplasmic reticulum Ca2+-ATPase: mechanisms of membrane protein insertion into liposomes during reconstitution procedures involving the use of detergents. *Biochim. Biophys. Acre* **1107**, 283–298 (1992).

56. Preus, S., Noer, S. L., Hildebrandt, L. L., Gudnason, D. & Birkedal, V. iSMS: single-molecule FRET microscopy software. *Nat. Methods* **12**, 593–594 (2015).

57. Hildebrandt, L. L., Preus, S. & Birkedal, V. Quantitative single molecule FRET efficiencies using TIRF microscopy. *Faraday Discuss.* **184**, (2015).

2. Haselwandter, C. A., Guo, Y. R., Fu, Z. & MacKinnon, R. Quantitative prediction and measurement of Piezo's membrane footprint. *Proc. Natl. Acad. Sci. U. S. A.* **119**, (2022).

3. Brohawn, S. G., Su, Z. & MacKinnon, R. Mechanosensitivity is mediated directly by the lipid membrane in TRAAK and TREK1 K+ channels. *Proc. Natl. Acad. Sci. U. S. A.* **111**, 3614–3619 (2014).

4. Cox, C. D., Bavi, N. & Martinac, B. Bacterial Mechanosensors. *Annu. Rev. Physiol.* **80**, 71–93 (2018).

5. Bavi, O. *et al.* Influence of Global and Local Membrane Curvature on Mechanosensitive Ion Channels: A Finite Element Approach. *Membranes (Basel).* **6**, 14 (2016).

6. Turner, M. S. & Sens, P. Gating-by-tilt of mechanically sensitive membrane channels. *Phys. Rev. Lett.* **93**, 118103 (2004).

7. Haselwandter, C. A., Guo, Y. R., Fu, Z. & MacKinnon, R. Elastic properties and shape of the Piezo dome underlying its mechanosensory function. *Proc. Natl. Acad. Sci. U. S. A.* **119**, (2022).

8. Markin, V. S. Lateral organization of membranes and cell shapes. *Biophys. J.* **36**, 1–19 (1981).

9. Corradi, V. *et al.* Lipid-Protein Interactions Are Unique Fingerprints for Membrane Proteins. *ACS Cent. Sci.* **4**, 709–717 (2018).

10. Schmidt, D. & MacKinnon, R. Voltage-dependent K+ channel gating and voltage sensor toxin sensitivity depend on the mechanical state of the lipid membrane. *Proc. Natl. Acad. Sci. U. S. A.* **105**, 19276–19281 (2008).

11. Aimon, S. *et al.* Membrane Shape Modulates Transmembrane Protein Distribution. *Dev. Cell* **28**, 212–218 (2014).

12. Quemeneur, F. *et al.* Shape matters in protein mobility within membranes. *Proc. Natl. Acad. Sci.* **111**, 5083–5087 (2014).

13. Kluge, C., Pöhnl, M. & Böckmann, R. A. Spontaneous local membrane curvature induced by transmembrane proteins. *Biophys. J.* **121**, 671–683 (2022).

14. Locher, K. P. Mechanistic diversity in ATP-binding cassette (ABC) transporters. *Nat. Struct. Mol. Biol.* **23**, 487–93 (2016).

15. Vasiliou, V., Vasiliou, K. & Nebert, D. W. Human ATP-binding cassette (ABC) transporter family. *Hum. Genomics* **3**, 281–290 (2009).

16. Januliene, D. & Moeller, A. Cryo-EM of ABC transporters: an ice-cold solution to everything? *FEBS Lett.* **594**, 3776–3789 (2020).

733 17. Thomas, C. *et al.* Structural and functional diversity calls for a new classification of ABC
734 transporters. *FEBS Lett.* **594**, 3767–3775 (2020).

735 18. Orelle, C., Schmitt, L. & Jault, J. Waste or die : The price to pay to stay alive. *Trends Microbiol.*
736 **31**, 233–241 (2022).

737 19. Chaptal, V. *et al.* Substrate-bound and substrate-free outward-facing structures of a multidrug
738 ABC exporter. *Sci. Adv.* **8**, 1–11 (2022).

739 20. Fribourg, P. F. *et al.* 3D cryo-electron reconstruction of BmrA, a bacterial multidrug ABC
740 transporter in an inward-facing conformation and in a lipidic environment. *J. Mol. Biol.* **426**,
741 2059–2069 (2014).

742 21. Orelle, C. *et al.* Conformational change induced by ATP binding in the multidrug ATP-binding
743 cassette transporter BmrA. *Biochemistry* **47**, 2404–2412 (2008).

744 22. Di Cesare, M. *et al.* The transport activity of the multidrug ABC transporter BmrA does not
745 require a wide separation of the nucleotide-binding domains. *J. Biol. Chem.* 105546 (2023).
746 doi:10.1016/j.jbc.2023.105546

747 23. Lewinson, O., Orelle, C. & Seeger, M. A. Structures of ABC transporters: handle with care.
748 *FEBS Lett.* **594**, 3799–3814 (2020).

749 24. Tang, Q. *et al.* Asymmetric conformations and lipid interactions shape the ATP-coupled cycle
750 of a heterodimeric ABC transporter. *Nat. Commun.* **14**, (2023).

751 25. Zoghbi, M. E. & Altenberg, G. A. Luminescence resonance energy transfer spectroscopy of
752 ATP-binding cassette proteins. *Biochim. Biophys. Acta - Biomembr.* **1860**, 854–867 (2018).

753 26. Husada, F. *et al.* Conformational dynamics of the ABC transporter McjD seen by single-
754 molecule FRET. *EMBO J.* **37**, e100056 (2018).

755 27. Verhalen, B. *et al.* Energy transduction and alternating access of the mammalian ABC
756 transporter P-glycoprotein. *Nature* **543**, 738–741 (2017).

757 28. Zoghbi, M. E. *et al.* Substrate-induced conformational changes in the nucleotide-binding
758 domains of lipid bilayer-associated P-glycoprotein during ATP hydrolysis. *J. Biol. Chem.* **292**,
759 20412–20424 (2017).

760 29. Wang, L. *et al.* Characterization of the kinetic cycle of an ABC transporter by single-molecule
761 and cryo-EM analyses. *Elife* **9**, 1–20 (2020).

762 30. Mehmood, S. *et al.* Structural and functional basis for lipid synergy on the activity of the
763 antibacterial peptide ABC transporter McjD. *J. Biol. Chem.* **291**, 21656–21668 (2016).

764 31. Steinfels, E. *et al.* Characterization of YvcC (BmrA), a multidrug ABC transporter constitutively
765 expressed in Bacillus subtilis. *Biochemistry* **43**, 7491–7502 (2004).

766 32. Mi, W. *et al.* Structural basis of MsbA-mediated lipopolysaccharide transport. *Nature* **549**, 233–
767 237 (2017).

768 33. Kapanidis, A. N. *et al.* Fluorescence-aided molecule sorting: analysis of structure and
769 interactions by alternating-laser excitation of single molecules. *Proc. Natl. Acad. Sci. U. S. A.*
770 **101**, 8936–41 (2004).

771 34. Deniz, A. A. *et al.* Single-pair fluorescence resonance energy transfer on freely diffusing
772 molecules: observation of Förster distance dependence and subpopulations. *Proc. Natl. Acad.*
773 *Sci. U. S. A.* **96**, 3670–5 (1999).

774 35. Hellenkamp, B. *et al.* Precision and accuracy of single-molecule FRET measurements—a multi-
775 laboratory benchmark study. *Nat. Methods* **15**, 669–676 (2018).

36. Selvin, P. R. & Ha, T. *Single-molecule Techniques: A Laboratory Manual*. *CSHL Press* (2008).

37. Lee, W., Von Hippel, P. H. & Marcus, A. H. Internally labeled Cy3/Cy5 DNA constructs show greatly enhanced photo-stability in single-molecule FRET experiments. *Nucleic Acids Res.* **42**, 5967–5977 (2014).

38. Lacabanne, D. *et al.* ATP Analogues for Structural Investigations: Case Studies of a DnaB Helicase and an ABC Transporter. *Molecules* **25**, (2020).

39. Javed, W. *et al.* Structural Insights into the Catalytic Cycle of a Bacterial Multidrug ABC Efflux Pump. *J. Mol. Biol.* **434**, (2022).

40. Li, M. J., Nath, A. & Atkins, W. M. Differential Coupling of Binding, ATP Hydrolysis, and Transport of Fluorescent Probes with P-Glycoprotein in Lipid Nanodiscs. *Biochemistry* **56**, 2506–2517 (2017).

41. Yan, Q., Shen, Y. & Yang, X. Cryo-EM structure of AMP-PNP-bound human mitochondrial ATP-binding cassette transporter ABCB7. *J. Struct. Biol.* **214**, (2022).

42. Marsh, D. Elastic curvature constants of lipid monolayers and bilayers. *Chem. Phys. Lipids* **144**, 146–159 (2006).

43. Liu, Y., Liu, Y., He, L., Zhao, Y. & Zhang, X. C. Single-molecule fluorescence studies on the conformational change of the ABC transporter MsbA. *Biophys. Reports* **4**, 153–165 (2018).

44. Tassis, K. *et al.* Single-molecule studies of conformational states and dynamics in the ABC importer OpuA. *FEBS Lett.* **595**, 717–734 (2021).

45. Yang, M. *et al.* Single-molecule probing of the conformational homogeneity of the ABC transporter BtuCD. *Nat. Chem. Biol.* **14**, 715–722 (2018).

46. Moeller, A. *et al.* Distinct Conformational Spectrum of Homologous Multidrug ABC Transporters. *Structure* **23**, 450–460 (2015).

47. Ambudkar, S. V., Cardarelli, C. O., Pashinsky, I. & Stein, W. D. Relation between the turnover number for vinblastine transport and for vinblastine-stimulated ATP hydrolysis by human P-glycoprotein. *J. Biol. Chem.* **272**, 21160–21166 (1997).

48. Levring, J. *et al.* CFTR function, pathology and pharmacology at single-molecule resolution. *Nature* **616**, 606–614 (2023).

49. Rigaud, J.-L. *et al.* Bio-Beads: an efficient strategy for two-dimensional crystallization of membrane proteins. *J. Struct. Biol.* **118**, 226–235 (1997).

50. Rigaud, J. L. & Lévy, D. Reconstitution of Membrane Proteins into Liposomes. *Methods Enzymol.* **372**, 65–86 (2003).

51. Rigaud, J. L., Pitard, B. & Levy, D. Reconstitution of membrane proteins into liposomes: application to energy-transducing membrane proteins. *BBA - Bioenerg.* **1231**, 223–246 (1995).

52. Lévy, D., Bluzat, A., Seigneuret, M. & Rigaud, J. L. A systematic study of liposome and proteoliposome reconstitution involving Bio-Bead-mediated Triton X-100 removal. *BBA - Biomembr.* **105**, 179–190 (1990).

53. Rigaud, J.-L., Lévy, D., G, M. & Lambert, O. Detergent removal by Bio-Beads. Application to membrane protein reconstitution and two-dimensional crystallisation. *Eur J. Biophys.* **27**, 305–319 (1998).

54. Mesmin, B. *et al.* XA four-step cycle driven by PI(4)P hydrolysis directs sterol/PI(4)P exchange by the ER-Golgi Tether OSBP. *Cell* **155**, 830 (2013).

55. Lévy, D., Guiik, A., Bluzat, A. & Rigaud, J.-L. Reconstitution of the sarcoplasmic reticulum

Ca2+-ATPase: mechanisms of membrane protein insertion into liposomes during reconstitution procedures involving the use of detergents. *Biochim. Biophys. Acre* **1107**, 283–298 (1992).

56. Preus, S., Noer, S. L., Hildebrandt, L. L., Gudnason, D. & Birkedal, V. iSMS: single-molecule FRET microscopy software. *Nat. Methods* **12**, 593–594 (2015).

57. Hildebrandt, L. L., Preus, S. & Birkedal, V. Quantitative single molecule FRET efficiencies using TIRF microscopy. *Faraday Discuss.* **184**, (2015).

Acknowledgements

We thank Raju Regmi, Elie Balloul and Nikos Hatzakis (University of Copenhagen) for support for the data analysis and insightful discussions. We thank Julien Maufront for analysis of the cryo-images of proteoliposomes. We thank Bassam Hajj, Julien Pernier and Xavier Solinas (Ecole Polytechnique) for technical support and David Lacoste (ESPCI), Peter Tieleman, Estefania Barreta Ojeda (University of Calgary) for providing conceptual ideas.
PB is member of the CNRS consortium AQV. AD, SJP, MD, PS, DL and PB are members of the Labex Cell(n)Scale (ANR-11-LABX0038) and Paris Sciences et Lettres (ANR-10-IDEX-0001-02). We acknowledge the Cell and Tissue Imaging Core facility (PICT IBiSA), Institut Curie, member of the French National Research Infrastructure France-BioImaging (ANR10-INBS-04).

Funding: This work was supported by:
Agence Nationale pour la Recherche : ANR-16-CE11-0026-01
Doctoral school EDPIF (ED564, Paris) for AD
Doctoral school ED CDV (ED 515, Paris) and PSL for SJP
Agence Nationale pour la Recherche : ANR-19-CE11-0002-01 for RKS and PS

Author contributions: MD, PB, DL and AD planned and designed the research. SJP, JM and DL purified the protein, optimized the liposome reconstitution. SJP, ADC and DL performed the cryo-EM images and ATPase activity measurements. AD and MD set up and optimized the single molecule FRET assay and sample preparation. AD performed the smFRET experiments and analysis. RKS and PS developed the theoretical model and performed the fit to the experimental data. AD, PB, DL and PS wrote the manuscript. EM and MC reviewed and commented on the manuscript.

Competing interests: Authors declare that they have no competing interests.

Data and materials availability: All data needed to evaluate the conclusions in the paper are present in the paper and/or the Supplementary Materials.

Figures and Tables

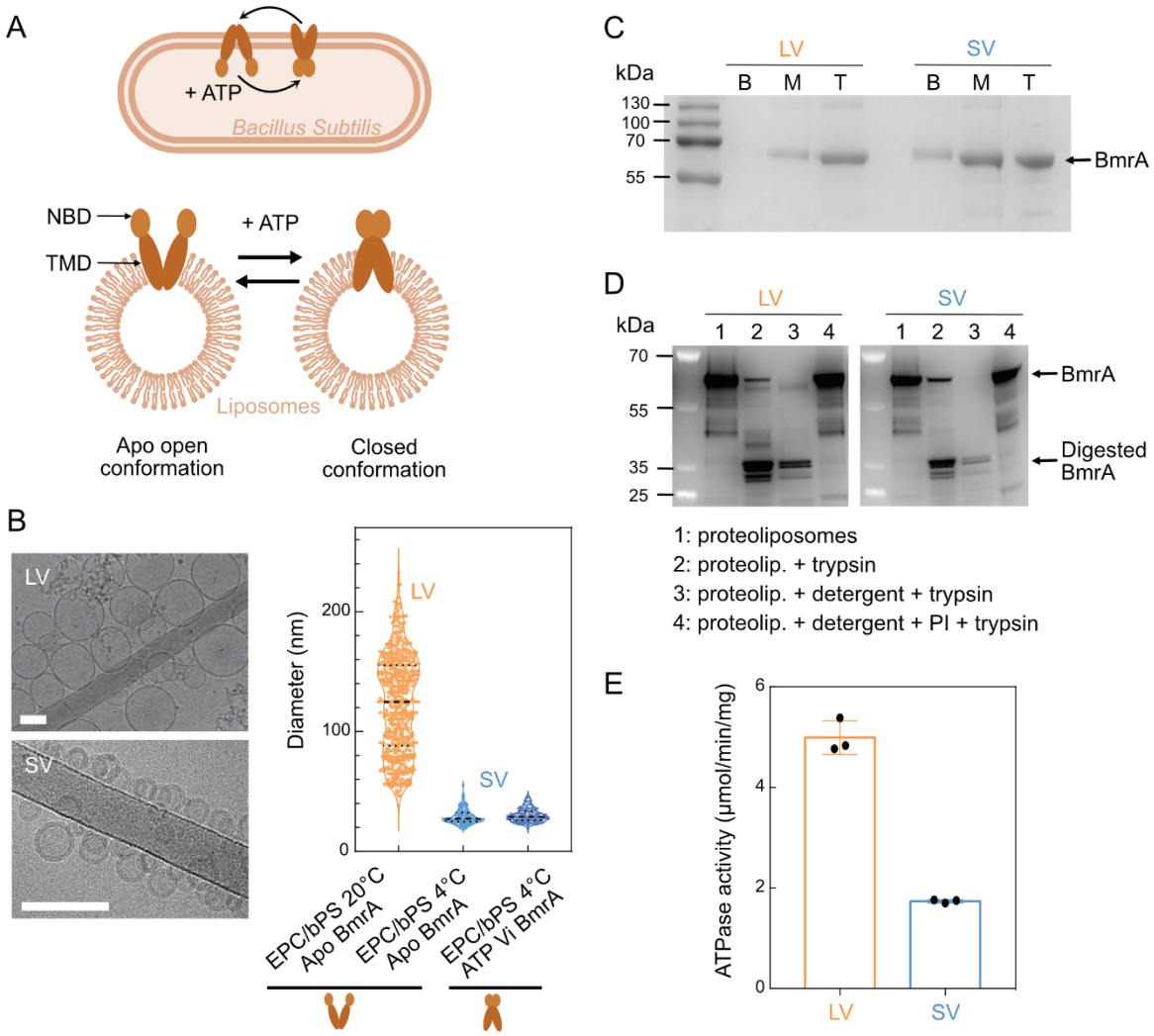

Figure 1. Increasing membrane curvature reduces BmrA ATPase activity. (A) Schematic representation of the two conformations of BmrA in *Bacillus Subtilis* (top) and reconstituted in opposite orientation in liposomes (bottom): the open or apo conformation (inward-facing in bacteria) and the closed conformation (outward-facing). **(B)** Left: Cryo-EM images of EPC:bPS (90:10 w/w) proteoliposomes (apo BmrA) obtained at two different reconstitution temperatures, T=20°C for the LV and T=4°C for the SV. Cryo-EM was used to characterize both the unilamellarity of the vesicles and their size distribution (scale bar: 50 nm). Right: Distribution of liposome sizes deduced from cryo-EM. Two different populations are obtained: average diameter ø=123 ± 41 nm (n = 594) for LV (Orange) and ø=29 ± 6 nm for SV, independently of the conformation of the protein incorporated, either open (apo, light blue, n=262) or closed (ATP Vi, dark blue, n=249). **(C)** Characterization of protein incorporation in vesicles LV (left) and SV (right) using a floatation assay in a sucrose gradient. Bottom (B), middle (M) and top (T) fractions are run on a NuPage gel. Intensity in the bottom fraction reveals very little protein aggregation, indicating that BmrA is properly incorporated in liposomes. **(D)** Characterization of protein orientation in vesicles LV (left) and SV (right), by cleaving the NBDs with trypsin. Alexa 488-labelled BmrA is reconstituted in LV or in SV, and the proteoliposome sample is run on the gel intact (1) and after 20 min incubation with 0.6 µg trypsin (2). Addition of detergent (det.) allows to resolubilize the proteoliposomes.This sample is run on the gel after 20 min incubation with 0.6 µg trypsin (3) and in presence of protease inhibitor (PI, used to stop the action of trypsin after 20min) and with 0.6 µg trypsin (4). Column 3 shows that solubilized BmrA is digested by trypsin. Column 4 reveals the efficiency of the protease inhibitor on trypsin. Column 2 shows that, both in LV and SV,

874 BmrA is 85% and 75%, respectively, oriented with NBD pointing outside. This characterization shows
875 that the protein has an orientation in liposomes opposite to bacteria (as represented in panel A). **(E)**
876 Effect of the liposome size on the protein ATPase activity (in µmol of ATP consumed per min per mg
877 of protein), in the presence of 5 mM of ATP at 37°C (3 measurements).

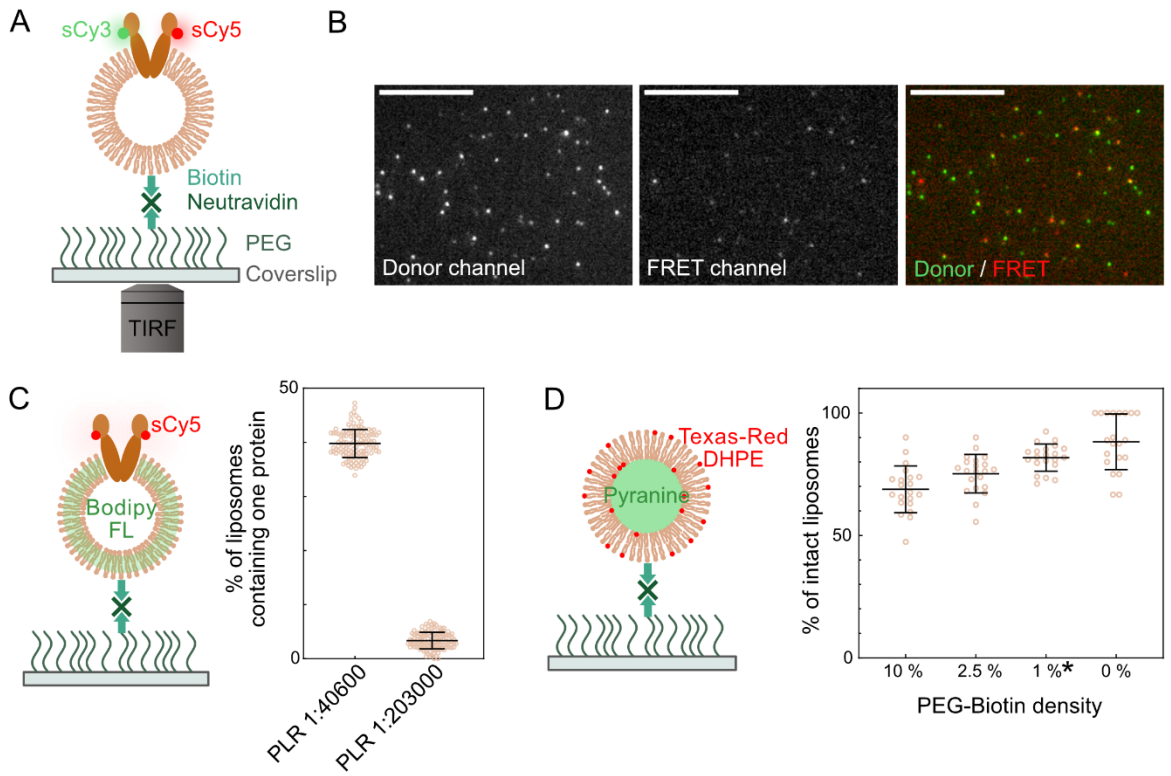

878 **Figure 2. Calibration and characterization of the smFRET assay. (A)** Scheme of smFRET with
879 BmrA labelled with sCy3 and sCy5 at C436, reconstituted in a liposome immobilized with neutravidine
880 on a coverslip passivated with PEG/PEG-biotin. **(B)** Typical TIRF-microscopy images showing the
881 Donor channel (Exc 532 nm Em 593 nm), the FRET channel (Exc 532 nm Em 684 nm), and the merge
882 (Donor: green and FRET: red). Scale bars: 10 µm. **(C)** Control of the single molecule regime in SV,
883 using a double labeling of the protein and of the liposome membrane. Left: Scheme of the experiment.
884 sCy5-labelled BmrA is reconstituted in SV that contain 0.01% fluorescent lipids (Bodipy®-FL).
885 Colocalization of sCy5 and Bodipy®-FL signals indicates a liposome containing at least one protein.
886 Right: Percentage of liposomes (per image) containing at least one BmrA, for two different PLR,
887 1:203000 and 1:40600. In both cases, most liposomes are empty. 120 images were analyzed. **(D)** Control
888 of the integrity of the liposomes after immobilization on the coverslip. Left: Liposomes containing 0.5%
889 DHPE-Texas Red® lipids and the soluble dye pyranine in their lumen are incubated for 5min in the
890 chamber. Potential rupture of the liposomes due to the adhesion via the PEG-biotin neutravidin
891 interaction is detected via the fluorescence signal: intact liposomes correspond to colocalization of the
892 green and red signals. Right: fraction of intact liposomes (per image) as a function of the PEG-biotin
893 density on the surface, 10, 2.5, 1 and 0%. The optimal condition is obtained at 1% (*), which has been
894 used in the whole study. 21 images were analyzed.

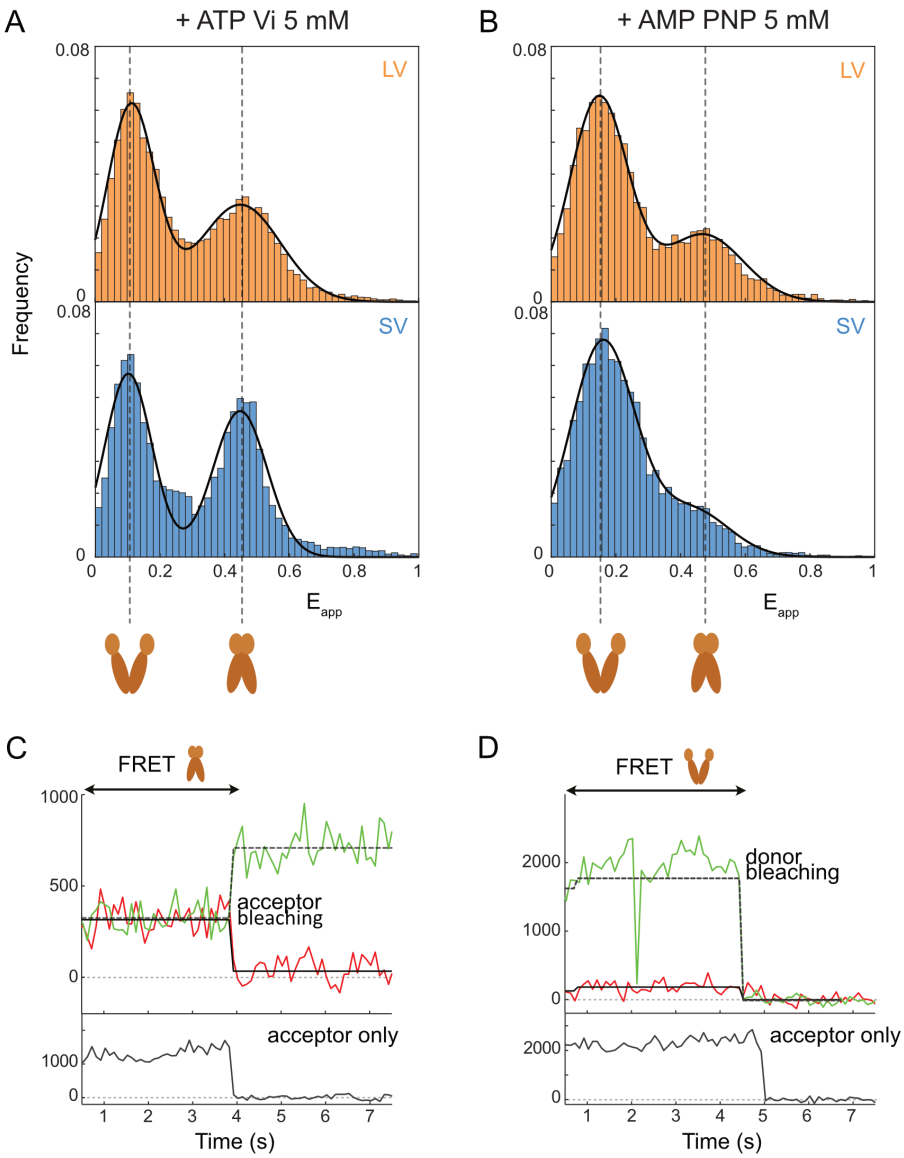

Figure 3. smFRET shows that BmrA closed conformation depends on membrane curvature in the presence of non-hydrolysable ATP. (A,B) Cumulated histograms of apparent FRET efficiency E_{app} upon addition of (A) ATP-Vanadate 5 mM in LV (top) and SV (bottom) (B) 5 mM AMPPNP in LV (top) and SV (bottom). The thick line corresponds to the two-gaussian fit. N_{all}: number of time points in histograms, N_{prot}: corresponding number of proteins. (A top) N_{all} = 18559 and N_{prot} = 525. (A bottom) N_{all} = 7552 and N_{prot} = 325. (B top) N_{all} = 5109 and N_{prot} = 157. (B bottom) N_{all} = 5094 and N_{prot} = 141. For each condition, data come from two independent experiments. **(C,D)** Typical time traces of proteins in LV with ATP-Vanadate 5mM (C) in closed state and (D) in open state. Top panel shows donor (green) and FRET (red) intensities over time. Plain and dashed line represent a fit of the FRET switches. Bottom panel shows the intensity of acceptor only (black).

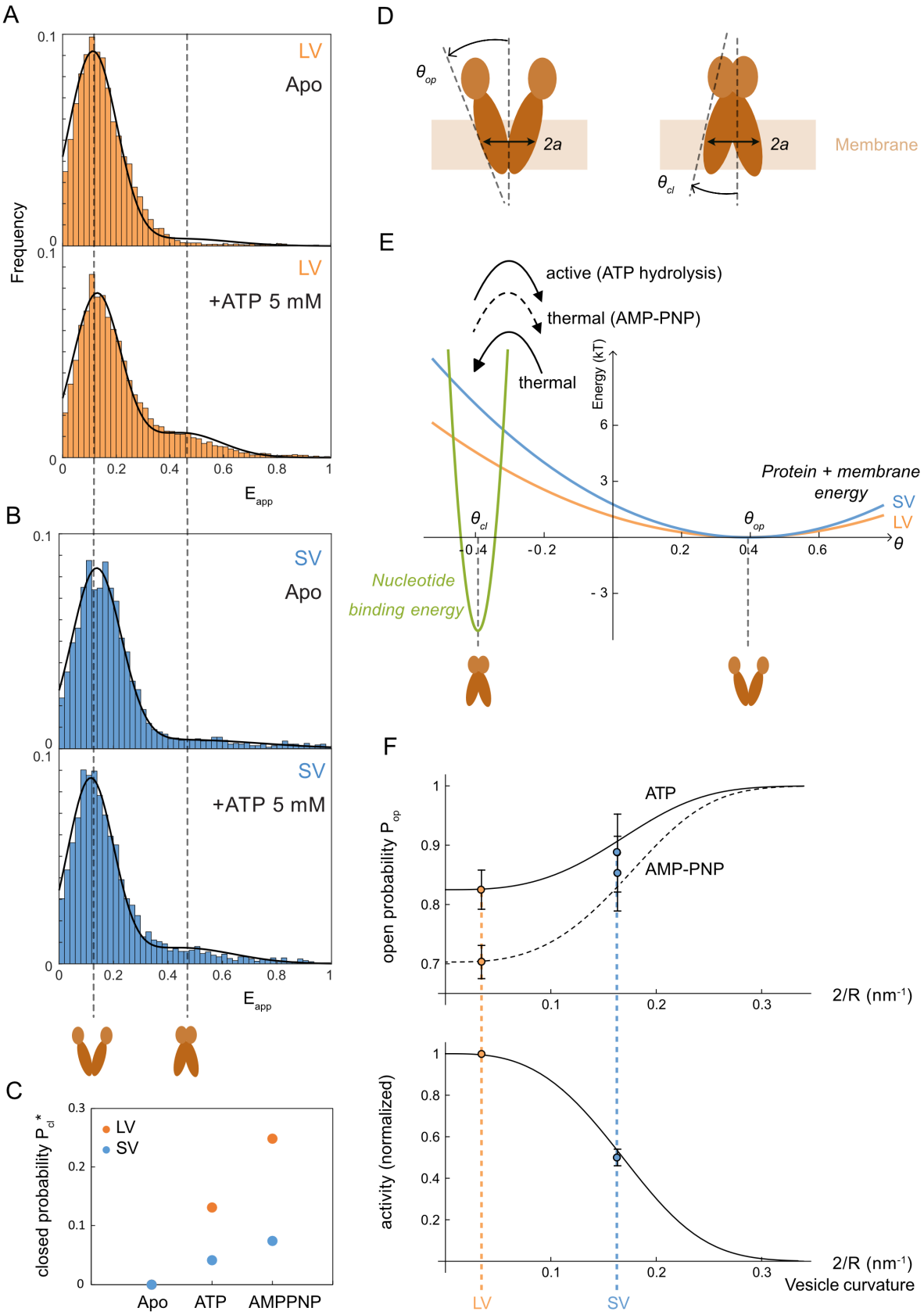

Figure 4. Effect of curvature on conformation and function of BmrA. (A,B) Cumulated histogram of apparent FRET efficiency E_{app} for BmrA in apo conformation in LV (top A) and SV (top B), and in

the presence of 5 mM Mg-ATP in LV (bottom A) and SV (bottom B). The thick line corresponds to a two-gaussian fit where the position of the high-FRET peak is set to $<E_{app}>_{HF}$ in ATP-Vanadate. (top A) N_{all} = 10451 and N_{prot} = 310. (bottom A) N_{all} = 7743 and N_{prot} = 226. (top B) N_{all} = 2797 and N_{prot} = 115. (bottom B) N_{all} = 3959 and N_{prot} = 130. For each condition, data come from two independent experiments, except SV Apo (top B) from three. **(C)** Probability for the protein to be in closed state P_{cl}* (P_{cl}* = P_{cl} – P_{cl}(apo) where P_{cl}(apo) corresponds to the high FRET fraction detected in apo state) as a function of nucleotide and liposome size. **(D)** Definition of the geometrical parameters 2a, θ_{op} and θ_{cl} used in the theoretical model. **(E)** Scheme of the two-state model. The energy landscape for the protein alone favors the open state. In the presence of nucleotides, NBDs dimerize, and an additional energy contribution (green) favors the closed state. The membrane energy adds a contribution that further disfavors the closed state, all the more as for the SV (blue) than for the LV (orange). The open-to-closed transition is thermal, while the closed-to-open is either thermal (non-hydrolysable AMP-PNP)) or triggered by ATP hydrolysis. **(F)** Results of the model for the probability of being in the open conformation (top, with ATP or AMP- PNP) and the activity (bottom, ATP turnover rate), as a function of the curvature of the SUVs. Dots corresponds to experimental data P_{op} from smFRET (top) and from ATPase assay (bottom). Both the opening probability and the activity curves were fitted with a single parameter κ=21 k_BT. Error bars are calculated by considering the high FRET Apo population as an uncertainty in the measurement.

		a_{LF}	$<E_{app}>_{LF}$	w_{LF}	a_{HF}	$<E_{app}>_{HF}$	w_{HF}
LV	ATP-Vi	0.062	0.11	0.10	0.030	0.45	0.18
	AMPPNP	0.064	0.15	0.13	0.021	0.47	0.17
	Apo	0.091	0.11	0.13	0.0034	0.45 (fix)	0.26
	ATP	0.077	0.13	0.13	0.012	0.45 (fix)	0.20
SV	ATP-Vi	0.058	0.10	0.10	0.046	0.45	0.12
	AMPPNP	0.067	0.16	0.14	0.015	0.43	0.16
	Apo	0.082	0.14	0.13	0.0042	0.45 (fix)	0.41
	ATP	0.085	0.12	0.12	0.0075	0.45 (fix)	0.27

Table 1. Two-gaussian fit parameters of BmrA smFRET histograms. Amplitude *a*, mean $<E_{app}>$, and width parameter *w* for the Low-FRET (LF) and High-FRET (HF) peaks.

		P_{op} (%)	P_{cl} (%)
LV	ATP-Vi	52.7 ± 0.3	47.3 ± 0.3
	AMPPNP	67.5 ± 1.5	32.5 ± 1.5
	Apo	92.3 ± 0.6	7.7 ± 0.6
	ATP	79.2 ± 0.9	20.8 ± 0.9
SV	ATP-Vi	50.3 ± 1.2	49.7 ± 1.2
	AMPPNP	78.9 ± 3.8	21.1 ± 3.8
	Apo	86.2 ± 0.7	13.8 ± 0.7
	ATP	82.1 ± 1.0	17.9 ± 1.0

Table 2. Fractions of proteins in open (*op*) and closed (*cl*) states for the two vesicle populations LV and SV. Calculated from the parameters of Table 1, the Low-FRET parameters correspond to the open conformation, and High-FRET to the closed state.